PHILOSOPHICAL TRANSACTIONS OF THE ROYAL SOCIETY A MATHEMATICAL, PHYSICAL & ENGINEERING SCIENCES

X-Ray Studies of Some Carbonized Coals

R. Diamond

Phil. Trans. R. Soc. Lond. A 1960 **252**, 193-223
doi: 10.1098/rsta.1960.0004

X-RAY STUDIES OF SOME CARBONIZED COALS

By R. DIAMOND*

Crystallographic Laboratory, Cavendish Laboratory, University of Cambridge

(*Communicated by Sir Charles Ellis, F.R.S.—Received* 19 *March* 1959)

CONTENTS

This paper describes the results obtained from an X-ray examination of the carbonization products of certain vitrain coals after treatment at temperatures up to 1000 °C. The methods employed in interpreting the X-ray data include a least-squares technique developed for the purpose of obtaining distributions of layer-sizes, and a Fourier transform technique developed by Hirsch (1954) to obtain distributions of the numbers of layers stacked parallel to one another. The importance of a number of secondary effects is examined, and the results are discussed in the light of these considerations.

1. Introduction

When the present work was begun, Hirsch's X-ray studies of raw coals were nearing completion (Hirsch 1954). The aim of Hirsch's work was to determine the structure of coal in as much detail as possible, since the micellar theory of Bangham, Franklin, Hirst & Maggs (1948), and the conclusions of Blayden, Gibson & Riley (1944) were both open to some doubt. The first of these was not based on conclusive data; Bangham's micellar theory was essentially a hypothesis based on considerations of the colloidal aspects and porosity of coal, and did not find support in Hirsch's work. The work of Blayden *et al.*, though less hypothetical in nature, proved to be subject to considerable errors in regard to the sizes of the layers and stacks of layers, their values being several times too large.

The present work extends Hirsch's studies into the field of carbonized coals; it corrects previous over-estimates of crystallite sizes, and provides more detailed information on the reactions involved in carbonization.

* Present address: Department of Physics, The Manchester College of Science and Technology, Manchester 1, England.

For a general review of the earlier X-ray work on coals and carbons the reader is referred to Hirsch (1954).

In two earlier papers (Diamond 1957, 1958*a*, hereinafter I and II) the computational methods employed in this work were described in detail. The present paper is concerned with the results obtained by these means and with their significance.

2. Specimens used, and their preparation

The four coals listed in table 1, all vitrains, have been carbonized *in vacuo* at a series of temperatures from 300 to 1000 °C. All the specimens used were hand-picked for low ash content by Dr G. W. Fenton and Mr J. W. Fowler of the Coal Survey Laboratory, Sheffield.

Table 1. The coals investigated

name	abbreviations	% carbon	% hydrogen	% volatile	type
Cannock Wood Shallow Seam	CW	80·5	5·1	40·0	low rank
Monk Bretton Meltonfield Seam	MM	84·4	5·3	38·5	caking coal
Roddymoor Ballarat Seam	RB	89·0	5·4	30·5	coking coal
Pontyberem Lower Pumpquart Seam	PQ	94·1	3·0	5·3	anthracite

The heat treatment consisted in an exponential rise in temperature towards an asymptotic value just greater than that at which the recording controller was set to equilibrate. The controller then held the specimen temperature constant within 5 °C at 1000 °C, and better at lower temperatures. The rise in temperature generally occupied about 3 h, irrespective of the final temperature attained, and the selected temperature was maintained for 3 h, after which the specimen returned exponentially, with a time constant of $2\frac{1}{4}$ h, to room temperature before examination.

Table 2. Concentrations of 'impurities'

coal	temperature (°C)	sulphur (%)	nitrogen (%)	chlorine (%)	ash (%)
Cannock Wood	200	1·98	0·89	0·80	—
	1000	0·35	0	0·56	0·42
Meltonfield	300	1·27	0·32	2·52	—
	1000	0·42	0	0·58	1·90
Roddymoor	200	1·25	0·72	0·27	—
	1000	0·57	0	0·38	0
Pumpquart	300	0·50	0·33	0·50	—
	1000	0·89	0	0·59	0

The percentage weight loss on carbonization, and the rate of increase of weight (by absorption of atmospheric gases) immediately after breaking the vacuum, were always recorded.

Digestion of the specimens under reflux with hydrochloric and hydrofluoric acids to remove mineral inclusions, was considered inadvisable on account of the undesirability of introducing chlorine as an impurity into the specimens and unnecessary since the specimens had been hand-picked for petrographic purity and (with two exceptions) showed no Debye–Scherrer lines from crystalline inclusions and very low ash contents on analysis (see table 2).

PHILOSOPHICAL TRANSACTIONS OF THE ROYAL SOCIETY A MATHEMATICAL, PHYSICAL & ENGINEERING SCIENCES

The specimens were prepared for the cameras by grinding to a fine powder, then adding just under 1% by weight of gum tragacanth, and distilled water. The resulting paste was formed into cylinders of diameter 0·8 mm by extrusion, for use in Debye–Scherrer vacuum cameras; and into slabs of 0·5 mm thickness for use in the low-angle focusing vacuum cameras. (The extrusion process was sufficiently easy-flowing to avoid producing any preferred orientation effects in the resulting specimens, which, unlike graphites, show little tendency to preferred orientation.) The diameter 0·8 mm (unusually large) is about optimum in these circumstances, since the scattering power and adsorption of carbon are both low ($\mu r = 0{\cdot}28$) and the scattering of X-rays by such materials as cokes is a sufficiently slowly varying function of scattering angle for this diameter of specimen to produce no significant modification of the observed intensity curve.

3. Studies at high angles

(*a*) *Experimental technique*

In the case of the high-angle studies ($(2 \sin\theta)/\lambda > 0{\cdot}4$ Å^{-1}) Cu $K\alpha$ radiation monochromatized by reflexion from a flat and undistorted single crystal of lithium fluoride was used in conjunction with an evacuated 9 cm Debye–Scherrer powder camera of the van Arkel type.

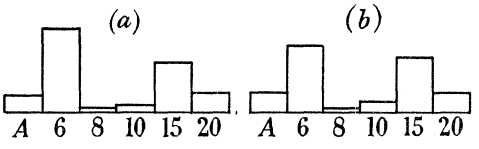

Figure 1. Two layer-size histograms from a single specimen. The numbers represent diameters in ångström units (L values), and the term marked A represents disordered or amorphous material. The ordinates are proportional to the fractions by weight of material in each size group. Histogram (*a*) was obtained by means of a light exposure and a shallow wedge, and (*b*) by means of a heavy exposure and a steep wedge.

Films thus obtained were photometered with a self-balancing photometer of the double-beam (Dobson) type, in which the density of each film was continuously compared with a wedge made from the same type of film, in which X-ray exposure (rather than optical density) was linear with distance; thus the position of the wedge at balance gave a direct reading of X-ray exposure.

The instrument was designed to scan the length of the film at constant velocity, simultaneously recording the wedge position on a paper chart moving in synchronism with the film. Measurements of intensity were taken from such charts at every 0·01 Å^{-1} in $s(s = (2 \sin\theta)/\lambda)$ by means of a calibration technique which was invariant with respect to film shrinkage in processing, and with respect to a rotation of the camera relative to the primary beam. This technique involved the use of a Perspex scale constructed for the purpose, the accuracy of which was closely checked against quartz, by means of the 2θ values given by Wilson & Lipson (1941). The errors revealed by this checking (1 to 2 parts per 1000) have been allowed for in the bond-length results quoted below.

Wedges of three different gradients were available, and, as a check, these were photometered against one another. All such tests substantiated the linearity of the wedges. In addition, a lightly and a heavily exposed photograph of the same specimen, photometered with shallow and steep wedges, yielded closely similar results (figure 1). For these reasons

it is held that the photometry is not a source of systematic error. Only two sources of error connected with photometry remain. The first of these is the random component due to hunting of the servo-system; this is such that a smooth mean line through the photometer trace has an indeterminacy of about $\frac{1}{2}$ %, which gives rise to fluctuations in the results obtained illustrated in figure 7 of II. The second source of error arises from the possibility of misplacing the origin of intensity; this effect is generally very slight when the margin of the film is photometered, and it gives rise to particular effects which are recognizable in the final results, if they are sufficiently serious to matter (see II).

(*b*) *Data processing*

The 31 intensity measurements in the range $0{\cdot}66 \leqslant s(\times 0{\cdot}01) \leqslant 0{\cdot}96$ Å^{-1}, which includes the (11) and (20) bands, were first divided by the polarization factor,

$$p = \frac{1+\cos^2 2\alpha \cos^2 2\theta}{1+\cos^2 2\alpha}, \tag{1}$$

in which α and θ are Bragg angles in monochromator and specimen, respectively. The resulting figures were then interpreted by the least-squares matrix method described earlier (II). Briefly, the method is as follows. Exact theoretical scattering functions, B, for graphitic layers of various sizes are arranged in a matrix $\mathbf{B}$, in which rows and columns correspond to size groups and s-values, respectively. A matrix $\mathbf{H}_f$, reciprocal to $\mathbf{B}$, is then calculated such that the product

$$\boldsymbol{\lambda} = \mathbf{H}_f \mathbf{I} \tag{2}$$

yields a distribution, in proportions by weight, of material in each of the specified layer-size groups, so that the linear combination of theoretical intensity functions $\mathbf{B}'\boldsymbol{\lambda}$ fits the observed intensities with minimum total square error. (The suffix, f, to $\mathbf{H}$ indicates the number of degrees of freedom allowed, which has been five throughout this work.) $\mathbf{I}$ is a column matrix containing the 31 observed intensities in order of ascending s-values.

Mean C—C bond lengths are also determined by the method already described in II, which utilizes the horizontal disregistry between observed and calculated intensity curves arising if the bond length is other than that assumed in computing the theoretical intensities.

(*c*) *Some tests of the method*

Before any appraisal of the results obtained can be attempted, it is necessary to test the methods employed in a number of ways. We must examine first the characteristics of the matrices employed; this has already been done in II. Secondly, we must examine the influence of various experimental factors, and thirdly we must examine the consequences of any inadequacies in the structural model in terms of which the scattering is interpreted. A detailed description of every test carried out is not given here; only the conclusions arrived at are quoted, full details being available elsewhere (Diamond 1956). In general, such tests are carried out by computing theoretical intensity figures which incorporate the influence of the effect to be studied, and then analyzing these by the matrices of II. The method is thus one of imitation. Further experimental tests using standard substances have recently been carried out by Ruland (1959).

The effect of fluorescent radiation has already been studied in II, and a test of the photometry has already been quoted. Of the remaining experimental factors, only two need be reported here. First, the monochromator employed was assumed to be a mosaic

crystal; if this assumption is incorrect, and the monochromator was a perfect crystal, which is most unlikely, then the bi-modal nature of some of the histograms obtained should be intensified. Secondly, measurements made with Mo $K\alpha$ radiation were in good agreement with those (normally used in the interpretation) obtained from Cu $K\alpha$ radiation; this would not be the case if, for example, iron impurities were present and fluorescing in the Cu $K\alpha$ radiation.

With regard to inadequacies in the structural model employed, tests have been performed to estimate the effects of over-size layers, thermal vibrations, aliphatic edge groups; five-membered rings and other bridges between layers, holes in large layers, elongated molecules and 'foreign' atoms. Tests relating to the degree of perfection of the layers have also been made, and will be referred to in § (*e*). We now take the others in order.

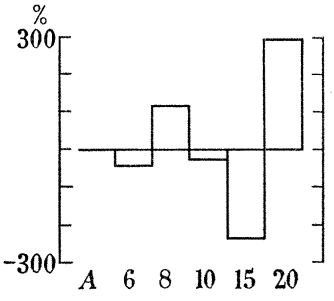

FIGURE 2. The analysis of theoretical intensity figures for $L = 30$ Å using a matrix for which $L = 20$ Å is the largest size-group available.

(i) *Oversize layers*

Figure 2 shows an analysis of theoretical data for $L = 30$ Å* using an earlier set of matrices (not published) for which $L = 20$ Å is the largest size-group for which provision was made. Evidently the sharp peak for $L = 30$ is best matched by an excess of the sharpest peak available (20 Å) minus a compensating amount of the 15 Å size-group which is somewhat less sharp. The effect is very characteristic, and may clearly be recognized when it occurs.

(ii) *Thermal vibrations*

This effect may be studied by replacing $J(s)$ of paper I by $1+[J(s)-1]\,e^{-Ks^2}$ to calculate the scattering when thermal vibrations are operative. The effect of this is to add a term given approximately by $1-e^{-0.58K}$ to the amorphous term, and to scale down the rest of the histogram by a factor $e^{-0.58K}$, almost without distortion. On the basis of Bacon's figures for graphite (Bacon 1952) the constant K has the value 0·065 Å^2 for the reflexions employed, whence a maximum of about 3 % of the material may appear to be amorphous from this cause. Conversely, the experimental values for the amorphous term obtained from the high-temperature specimens indicate an upper limit of 0·1 Å^2 for K, supposing these terms to be entirely due to this effect.

(iii) *Aliphatic edge groups*

If we enlarge the molecules used in I by the addition of carbon atoms singly bonded at all available edge positions, with a bond length of 1·53 Å, we may calculate the X-ray

* L is an effective diameter of the 'layers' (condensed aromatic ring systems). In ångströms, L is given by $L=2{\cdot}5\sqrt{(\frac{1}{2}N)}$ where N = number of C atoms in the layer, see I.

scattering from such molecules and analyze this by the method of II to determine the effect of the first members of aliphatic side chains. This has been done for classes 3 and 9 of I ($L = 8{\cdot}4$ and 20 Å, respectively). Second members of aliphatic side chains are considered to be so arbitrarily displaced from the nearest lattice sites (corresponding to an extension of the aromatic nucleus) as to contribute only to the amorphous scattering.

The results of such investigations show that in the case of the smaller molecules ($L = 8{\cdot}4$ Å), such first side-chain atoms contribute to the amorphous material apparently present to just half the extent to be expected if they were entirely randomly sited, and that they also contribute to the apparent layer size to the same extent as if they were bonded

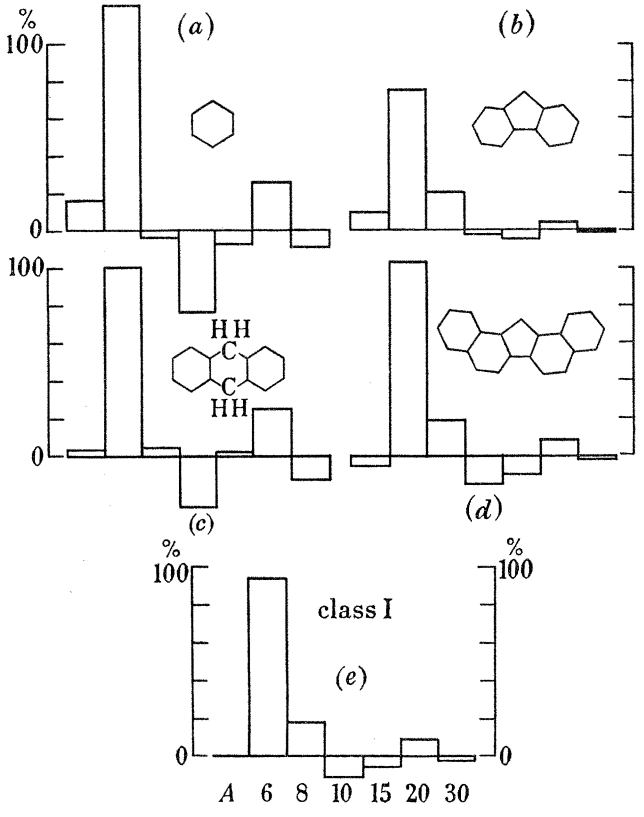

FIGURE 3. The effects of some special molecules. For explanation see text.

to the aromatic nucleus by aromatic instead of aliphatic bonds. For the larger molecules ($L = 20$ Å) such atoms contribute to the amorphous term by 38% of their weight, instead of 50%, and again contribute totally to the apparent layer size.

(iv) *Five-membered rings and hydro-aromatic bridges*

Computations similar to the above have been carried through to estimate the influence of five-membered rings and hydroaromatic groupings occurring as bridges between two otherwise perfect aromatic fragments, the results are illustrated in figure 3.

Figure 3*a* shows an analysis of a set of theoretical scattering data for benzene, which should be compared with the distribution of figure 3*e* which corresponds to 100% of the 5·8 Å size-group. The strong negative and positive terms in the centre and right of this distribution are partly due to the fact that benzene is smaller than the smallest aromatic

size-group, the situation thus being analogous to that of figure 2, and are partly also a characteristic of a narrow size distribution (cf. figure 5 of II). Evidently this distribution has a large ϵ component† (see II), and it is possible, therefore that single ring groupings may be contributing to this vector in experimental cases where this appears large.

The molecule of figure 3*b* (the carbon skeleton of fluorene) has an analysis very closely similar to those obtained from some coals treated at about 500 °C. We may conclude, therefore, that the X-ray method cannot detect five-membered rings in very small molecules, since their effect must be masked by the similar effect arising from normal small aromatic molecules. This molecule does, however, show the effects of its irregularity in that its apparent mean layer size corresponds to 11·5 atoms though it contains 13 atoms.

If, however, a five-membered ring occurs in a rather larger molecule, such as that of figure 3*d*, we see from the close resemblance of its histogram to that of class 1 (figure 3*e*) that the departures from a hexagonal lattice are sufficiently large for the two naphthalene residues to diffract independently, there being no definite phase relationship between them. Similarly, the molecule of figure 3*c* having a double —CH_2— non-planar bridge, also diffracts like two *ortho*-xylene residues since its histogram is intermediate between those of figures 3*a* and *e* (being nearer to the former); whereas, if it were planar and regular, it would appear a little larger than class 1.

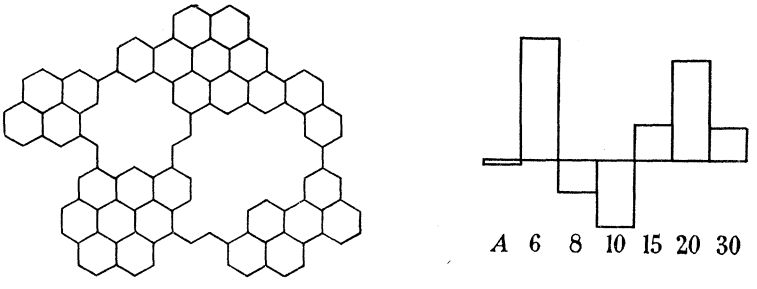

FIGURE 4. The influence of holes in large layers.

We therefore draw the important conclusions that wherever a non-planar hydroaromatic bridge or five-membered ring separates two perfect aromatic fragments, the molecule is effectively terminated for X-ray purposes, and the two parts contribute independently to the histogram, except in the case of the smallest molecule shown (fluorene) where the effect is only partial.

I am particularly indebted to Dr P. B. Hirsch for the $J(s)$ values from which the histograms of *b*, *c* and *d* were derived.

(v) *Holes in large layers*

In order to investigate the effect of vacant sites in large layers, eighteen atoms were removed from one of the configurations used in I to obtain the theoretical intensity curves for $L = 20$ Å. The modified configuration, containing two holes of sizes comparable to the molecules used to calculate the 5·8 Å theoretical intensity curve, is shown in figure 4 together with the distribution to which it gives rise. The effect is an example of Babinet's principle, in that the holes give rise to diffraction effects interpretable as scattering from

† The histograms are made up of a number of mathematically independent components (eigenvectors) of which the ϵ component is the least accurate.

layers of the same size as the holes. For present purposes, however, it is more important to note that the bi-modal nature of the histograms obtained from some of the high-temperature cokes is quite consistent with the existence of this effect, to a limited extent; we shall return to this point in our discussion.

It is also important to note that the present calculations assume that the remaining atoms still lie exactly on the lattice sites of a single regular lattice. In the case of cokes, however, if it is supposed that such configurations are produced as a result of layer growth, it is unlikely that this assumption would be exactly satisfied; the terms corresponding to the small layers would then be further enhanced at the expense of the terms for the large layers.

(vi) *Elongated molecules*

The diffraction effects produced by a molecule with length more than twice its breadth have also been studied.

Figure 5*a* shows the molecule and its histogram, which may be compared with 5*b* which is the histogram for a compact molecule with the same number of atoms. The relative broadening in the former case is quite apparent. The experimental histograms presented in the next section frequently show wide distributions, but not generally of this type. This is consistent with the view that the molecules present in coal are, in the main, isodimensional.

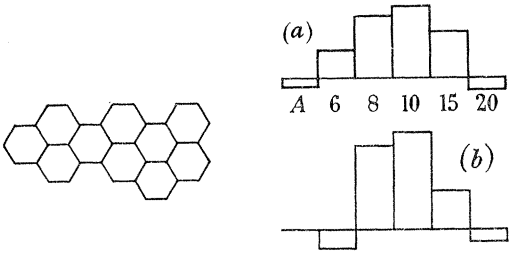

FIGURE 5. The effects of an elongated molecule.

(vii) *The influence of 'foreign' atoms, and of a revision in the figures for Compton scattering*

In the development of the method described in II, the possible presence of non-carbon atoms was ignored, it being assumed that the scattering from such atoms could be regarded as single-atom scattering having the form f^2+C. It was further assumed that this function would be in a constant ratio to the corresponding function for carbon for any foreign atoms likely to be present; in which case such atoms would contribute to the amorphous term in the histograms only, and with a weighting factor similar to the ratio of the atomic weight of the element concerned to that of carbon.

The first of these assumptions is difficult to examine critically, as the structural role of non-carbon atoms is not exactly known. For those non-carbon atoms in side chains, other than the first members of such side chains, the assumption is probably quite good enough, but for those which are hetero-atoms within the layers, or which form the first members of side chains, the single-atom assumption is certainly not justified, and the contribution to the X-ray scattering is not simply f^2+C.

It was shown above, (iii), that the first members of aliphatic side chains contribute partially to the amorphous scattering and totally to the apparent layer size. Thus phenolic oxygen should appear in the histograms in the aromatic terms, and also in the amorphous

term to an extent depending on the size of the layer to which such oxygen is attached. It does not appear to be practicable to make a rigorous allowance for oxygen in this way, but we may still make a correction by assuming all such non-carbon atoms to give rise to single-atom scattering, and by ascribing them entirely to the amorphous term in the histogram, and then analyzing the remainder in terms of carbon scattering. Such a correction represents the maximum influence which such atoms may exert on the histograms, and it may then be said that the true layer-size distribution lies between the uncorrected and corrected distributions.

In evaluating this extreme correction we need no longer make the second assumption above, concerning the ratio of the scattering intensities of non-carbon and carbon atoms, and we may at the same time make allowance for the revised figures for the Compton scattering for carbon recently given by Keating & Vineyard (1956). On this basis we may proceed as follows for the case of hydrogen and oxygen as impurities; terms for other elements of the same algebraic form may be added if desired.

In the absence of interactions between atoms of different types, the observed X-ray intensity in arbitrary units may be written as

$$\mathbf{I} = K[n_{\mathrm{C}}\mathbf{I}_{\mathrm{C}}+n_{\mathrm{O}}\mathbf{I}_{\mathrm{O}}+n_{\mathrm{H}}\mathbf{I}_{\mathrm{H}}], \tag{3}$$

in which K is a scaling constant, $\mathbf{I}_{\mathrm{C}}$ is the true scattering from carbon in electron units, $\mathbf{I}_{\mathrm{O}}$ that from oxygen and $\mathbf{I}_{\mathrm{H}}$ that from hydrogen and n_{C}, n_{O} and n_{H} the fractions by number of these types of atom present in the specimen. We also write $\boldsymbol{\delta}$ as

$$\mathbf{C}_{\mathrm{CA}}-\mathbf{C}_{\mathrm{KV}} = \boldsymbol{\delta}, \tag{4}$$

being the difference between the Compton scattering figures as given by Compton & Allison (1935) and by Keating & Vineyard, then the true layer-size distribution for carbon is given by the product

$$\boldsymbol{\lambda}_{\mathrm{C}} = \mathbf{H}_f(\mathbf{I}_{\mathrm{C}}+\boldsymbol{\delta}), \tag{5}$$

since the matrices are appropriate if the observations are made to simulate those which would be obtained if Compton & Allison's figures were correct. This leads to

$$\frac{\boldsymbol{\lambda}_{\mathrm{C}}}{\Sigma\lambda_{\mathrm{C}}} = \frac{\boldsymbol{\lambda}}{\Sigma\lambda}(1-\Sigma\lambda_{\delta})+\boldsymbol{\lambda}_{\delta}+\frac{n_{\mathrm{O}}}{n_{\mathrm{C}}}\left[\boldsymbol{\lambda}\frac{\Sigma\lambda_{\mathrm{O}}}{\Sigma\lambda}-\boldsymbol{\lambda}_{\mathrm{O}}\right]+\frac{n_{\mathrm{H}}}{n_{\mathrm{C}}}\left[\boldsymbol{\lambda}\frac{\Sigma\lambda_{\mathrm{H}}}{\Sigma\lambda}-\boldsymbol{\lambda}_{\mathrm{H}}\right], \tag{6}$$

in which

$$\left.\begin{aligned}\boldsymbol{\lambda}_{\delta} &= \mathbf{H}_f(\mathbf{C}_{\mathrm{CA}}-\mathbf{C}_{\mathrm{KV}}),\\ \boldsymbol{\lambda}_{\mathrm{O}} &= \mathbf{H}_f\mathbf{I}_{\mathrm{O}},\\ \boldsymbol{\lambda}_{\mathrm{H}} &= \mathbf{H}_f\mathbf{I}_{\mathrm{H}},\end{aligned}\right\} \tag{7}$$

and $\boldsymbol{\lambda}$ is the distribution obtained experimentally before making adjustments for these effects. The resulting distribution corresponds to that for the carbon alone in the absence of interaction between carbon and non-carbon atoms.

With the assumption of gas-like scattering from O and H, I_{O} is $f_{\mathrm{O}}^2+C_{\mathrm{O}}$ and I_{H} is unity, and the final corrected distribution may be obtained by multiplying $\boldsymbol{\lambda}_{\mathrm{C}}/\Sigma\lambda_{\mathrm{C}}$ by the weight per cent of carbon, and adding the weights per cent of oxygen and hydrogen to the amorphous term. (And multiplying the result by [1 − fraction of material evaporated] if results comparable to those of figure 6 are desired.)

Table 3 gives results in both corrected and uncorrected forms, and the correction vectors $\boldsymbol{\lambda}_\delta$, $\boldsymbol{\lambda}_O$ and $\boldsymbol{\lambda}_H$ are given in table 4, inspection of which shows (cf. figure 3 and matrix A of II) that the corrections for Compton scattering and for oxygen include a strong

TABLE 3

temp. (°C)	specimen	weight per cent: evaporated	amorphous: H	amorphous: O	amorphous: C	5·8 Å	8·4 Å	10 Å	15 Å	20 Å	30 Å	mean layer size (Å)
300	CW	16·0	—	—	25·0	50·0	9·0	−2·0	0·0	2·0	0·0	6·5
		*16·0	4·0	15·0	−0·3	57·6	10·2	−1·4	−1·5	0·0	0·3	
	MM	6·0	—	—	24·0	56·0	13·0	1·0	0·0	0·0	0·0	6·4
		*6·0	4·8	13·0	2·9	59·5	13·6	0·4	0·3	0·0	0·0	
	RB	1·5	—	—	16·5	50·0	22·0	10·0	0·0	0·0	0·0	7·15
		*1·5	5·3	6·5	8·5	44·4	21·6	11·3	1·2	0·0	−0·8	
	PQ	3·0	—	—	7·5	20·5	27·5	25·0	11·0	2·5	3·0	9·95
		3·0	2·7	6·5	1·7	16·6	27·1	26·0	11·3	1·9	2·5	
400	CW	25·0	—	—	19·0	39·0	14·0	3·0	−1·0	1·0	0·0	6·6
		*25·0	2·8	11·7	0·5	42·7	15·4	3·1	−2·1	0·0	0·7	
	MM	22·0	—	—	18·0	41·0	13·0	4·0	2·0	0·0	0·0	6·8
		*22·0	3·4	10·8	1·0	43·9	13·6	3·4	1·3	0·0	0·0	
	RB	11·0	—	—	16·0	51·0	14·0	4·0	4·0	0·0	0·0	7·15
		11·0	4·4	7·2	6·6	47·4	13·9	5·3	4·7	−0·4	−0·3	
	PQ	3·0	—	—	8·0	24·0	28·0	25·0	7·0	1·0	4·0	10·0
		*3·0	2·7	4·3	7·1	16·8	27·2	26·8	7·8	0·0	3·6	
500	CW	33·0	—	—	12·0	44·0	10·0	0·0	0·0	1·0	0·0	6·7
		*33·0	2·1	7·1	2·4	43·1	10·9	1·0	−0·4	0·0	0·5	
	MM	31·0	—	—	13·0	33·0	15·0	7·0	0·0	1·0	0·0	7·2
		*31·0	2·1	8·8	0·1	35·1	15·4	6·6	−0·5	1·0	0·1	
	RB	25·5	—	—	6·5	49·0	13·0	3·0	3·0	0·0	0·0	7·2
		25·5	2·6	6·6	−1·8	47·9	12·6	3·1	3·4	0·2	−0·5	
	PQ	3·5	—	—	8·5	21·0	26·0	25·0	11·0	3·0	2·0	10·05
		3·5	2·9	4·2	7·5	12·9	25·2	27·6	11·6	1·3	3·0	
600	CW	36·5	—	—	9·5	35·0	13·0	3·0	0·0	2·0	1·0	7·5
		36·5	1·4	6·6	0·9	36·5	12·4	1·9	0·2	2·8	0·5	
	MM	35·0	—	—	9·0	34·0	10·0	4·0	6·0	2·0	0·0	7·9
		35·0	1·5	7·7	−1·8	37·2	9·4	2·2	6·1	3·3	−0·7	
	RB	29·0	—	—	5·0	30·0	18·0	10·0	4·0	3·0	1·0	8·7
		29·0	2·0	6·6	−3·2	30·0	17·5	9·5	4·3	3·5	0·6	
	PQ	5·0	—	—	10·0	24·0	22·0	19·0	12·0	7·0	1·0	10·15
		5·0	2·6	5·3	6·7	18·2	21·9	20·7	12·4	5·9	1·0	
700	CW	38·5	—	—	8·5	30·0	11·0	3·0	3·0	5·0	1·0	9·1
		38·5	1·0	6·6	0·1	32·2	10·4	1·6	3·2	6·0	0·4	
	MM	37·0	—	—	8·0	21·0	13·0	8·0	7·0	6·0	0·0	9·6
		*37·0	1·0	7·9	−2·8	23·5	13·2	7·2	6·6	6·2	0·0	
	RB	31·0	—	—	5·0	25·0	17·0	12·0	4·0	3·0	3·0	9·7
		31·0	1·1	6·6	−2·8	26·1	16·4	10·9	4·2	3·8	2·5	
	PQ	6·0	—	—	11·0	15·0	18·0	19·0	15·0	12·0	4·0	11·3
		6·0	1·8	5·0	9·0	9·7	17·8	20·5	15·3	10·8	3·5	
800	CW	40·0	—	—	8·0	23·0	6·0	1·0	9·0	12·0	1·0	11·4
		40·0	0·8	5·5	1·9	23·7	5·5	0·3	9·1	12·5	0·7	
	MM	38·5	—	—	7·0	19·0	9·0	7·0	10·0	10·0	0·0	10·9
		*38·5	0·7	7·2	−1·1	20·2	9·0	6·4	9·6	10·0	0·0	
	RB	32·0	—	—	4·0	26·0	11·0	6·0	8·0	10·0	3·0	11·2
		32·0	0·7	4·0	2·1	23·0	10·7	6·7	8·2	9·5	2·8	
	PQ	7·0	—	—	11·0	5·0	17·0	21·0	16·0	11·0	12·0	14·65
		7·0	1·5	5·2	8·6	0·8	16·8	22·1	16·2	10·1	11·6	
900	CW	41·0	—	—	8·0	18·0	4·0	2·0	11·0	14·0	2·0	12·5
		41·0	0·6	4·0	5·2	16·4	3·9	2·3	11·1	14·3	1·8	
	MM	39·5	—	—	7·5	22·0	4·0	1·0	10·0	14·0	2·0	12·2
		39·5	0·6	5·2	2·3	22·3	3·7	0·4	10·1	14·4	1·6	
	RB	32·5	—	—	3·5	28·0	9·0	3·0	6·0	10·0	8·0	12·5
		32·5	0·3	2·7	4·8	23·1	8·3	4·6	7·3	8·9	7·8	
	PQ	†7·5	—	—	7·5	3·0	12·0	14·0	16·0	16·0	24·0	18·0
		‡†*7·5	0·7	4·6	6·9	0·0	11·4	14·4	16·4	15·5	22·7	
1000	CW	42·0	—	—	8·0	21·0	3·0	−1·0	10·0	15·0	2·0	12·9
		42·0	0·4	2·5	8·6	16·9	3·1	0·3	10·1	13·8	2·1	
	MM	40·0	—	—	7·0	14·0	5·0	4·0	12·0	15·0	3·0	13·6
		‡40·0	0·3	2·5	7·8	10·2	5·1	5·3	12·0	13·8	2·8	
	RB	32·5	—	—	0·5	24·0	5·0	0·0	10·0	18·0	10·0	14·8
		32·5	0·1	2·8	1·8	19·7	5·1	1·5	10·1	16·6	9·7	
	PQ	data not available										

* ϵ-vector adjustments made after the O, H and Compton scattering corrections.
† Only one set of X-ray data employed.
‡ Chemical analyses questionable.

ϵ component; for this reason, in some of the oxygen-rich specimens small alterations have been made to this component after making the main corrections. For example, for the Meltonfield 300 °C specimen, after the principal corrections have been applied the carbon terms read 2·5, 61·9, 12·1, −1·7, 1·0, 2·0, −1·2 which, with an ϵ adjustment also, become 2·9, 59·5, 13·6, 0·4, 0·3, 0·0, 0·0, the criterion for this adjustment being the smoothing of the small but physically unreasonable fluctuations in the terms for the larger layer sizes. The adjustments so made have all been very small, only the Cannock Wood 300 °C and 400° C adjustments being larger than those of this example.

TABLE 4. CORRECTION VECTORS FOR O, H AND COMPTON SCATTERING

size group / vector	amorphous (including pairs)	5·8 Å	8·4 Å	10 Å	15 Å	20 Å	30 Å	$\Sigma\lambda$
λ_δ	+0·1156	−0·1166	+0·0129	+0·0541	+0·0102	−0·0289	+0·0077	+0·0550
λ_O	+2·8092	−1·9826	+0·2793	+0·9758	+0·0934	−0·5933	+0·2091	+1·7911
λ_H	+0·0605	+0·0981	−0·0115	−0·0437	−0·0067	+0·0253	−0·0073	+0·1148

(*d*) *Results*

In this section are presented the results of the investigations at high angles; our discussion of them is deferred to the final section.

Table 3 gives the results obtained in numerical form. Two rows of figures appear for each specimen, the first being the average obtained from at least two independent determinations, but without making any special allowance for non-carbon atoms, or for the revision in Compton scattering figures. The second row of figures is in each case derived from the first in accordance with the revisions described in the previous section. Histograms of the unrevised results are also given in figure 6. Throughout these tables, and in the figure, the scaling is such that the sum of the terms, including the material evaporated, comes to 100 %, thus permitting direct correlation between one temperature and another. In computing the revised distributions the elementary analysis figures provided by Drs Weiler and Strauss of the Micro-Analytical Laboratory, Oxford, have been used, in which the oxygen content was obtained by difference. The figures for oxygen thus include the small amounts of sulphur, chlorine and nitrogen (table 2) which, for the purposes of this revision, need not be distinguished from oxygen in the concentrations in which they are present. In figure 7, we show the variation with temperature of the mean layer size, $\bar{L}$, given by $\Sigma\lambda L/\Sigma\lambda$, the non-aromatic term being omitted from the summation. Since the scattering curves, B, are expressed as scattered intensity per atom, this gives a weight average, not a number average.

Evidently, the three bituminous series have closely similar $\bar{L}$ values throughout the temperature range investigated, but with a slight tendency for them to be resolved in order of rank, with the implication that above 1000 °C this resolution may become more marked. At 300 °C these three series differ mainly in the proportion of amorphous material; the Roddymoor has, however, a slightly larger layer diameter. With an increase in temperature we find volatilization taking place primarily at the expense of the amorphous term, which falls to a steady value, followed generally by some reduction in the 5·8 Å term. Growth generally begins between 500 and 600 °C and continues almost linearly with

PHILOSOPHICAL TRANSACTIONS OF THE ROYAL SOCIETY A MATHEMATICAL, PHYSICAL & ENGINEERING SCIENCES

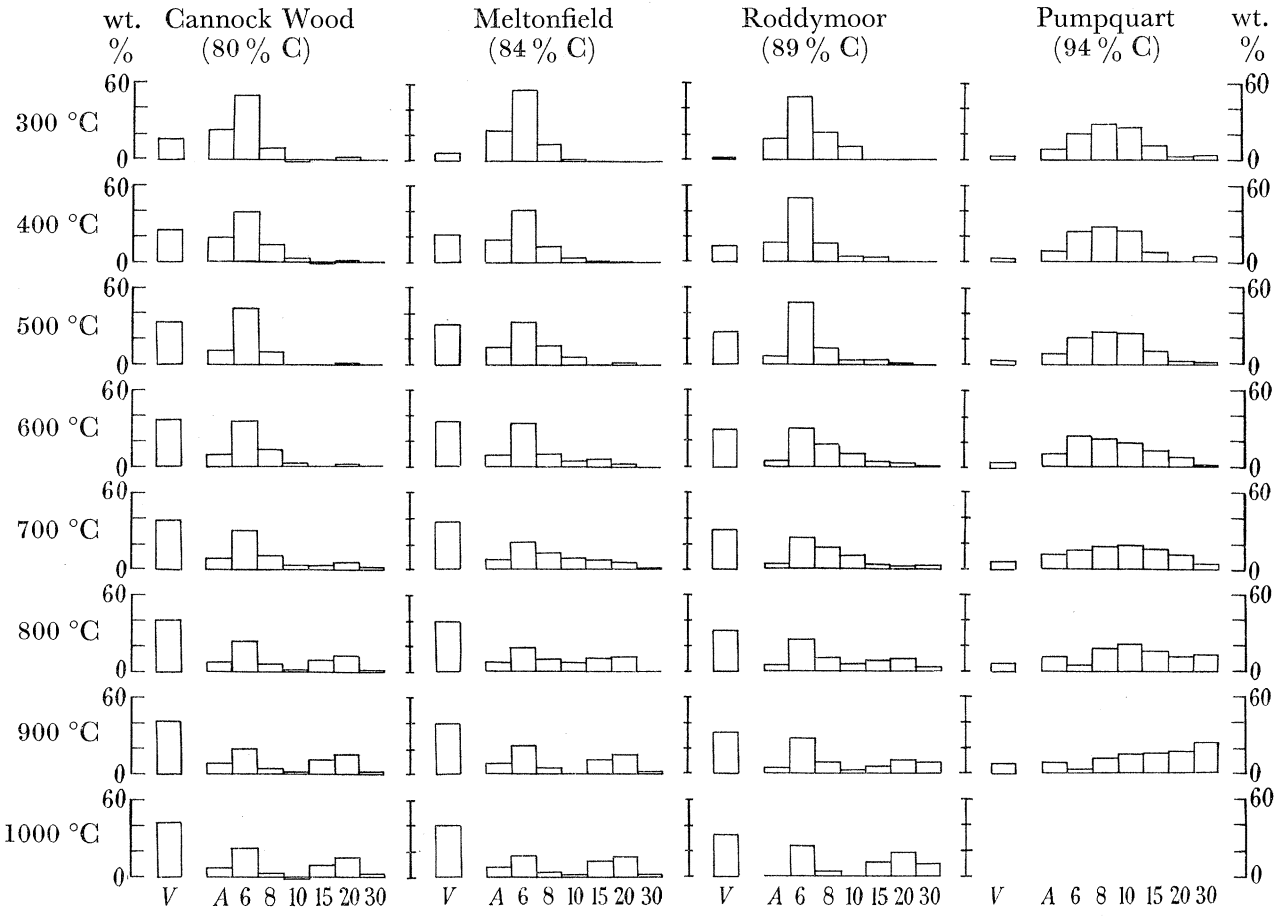

FIGURE 6. Layer size histograms for four carbonized vitrains. The layer sizes in ångström units are indicated at the foot of the figure, the size group *A* being amorphous (single) atoms, and *V* is the amount of material evaporated at the temperature indicated. The sum of the terms, including *V*, comes to 100 %.

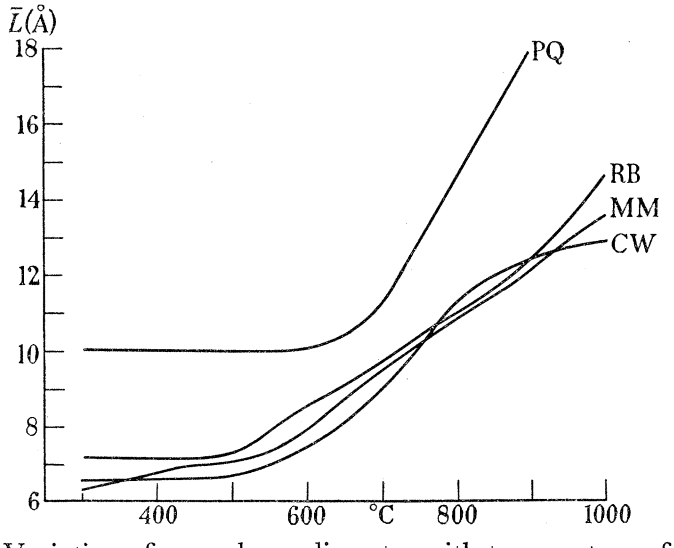

FIGURE 7. Variation of mean layer diameter with temperature of treatment.

temperature up to 1000 °C; this is thought to take place by the coalescence of small layers, but the indications are that not all the small layers succeed in growing, some 10 or 20% persisting at 1000 °C. Studies of factors influencing the bi-modality of the high temperature histograms (e.g. polarization factor and (20) band referred to in II) tend to support the view that this bi-modality is genuine.

The Pumpquart (anthracite) series differs markedly from the other three in showing a broad distribution of layer sizes at all temperatures. Variations in $\bar{L}$ show a delayed onset in growth, followed by a more rapid growth than in the bituminous series. The histograms also show that in this series the smallest layers have almost entirely vanished by 900 °C.

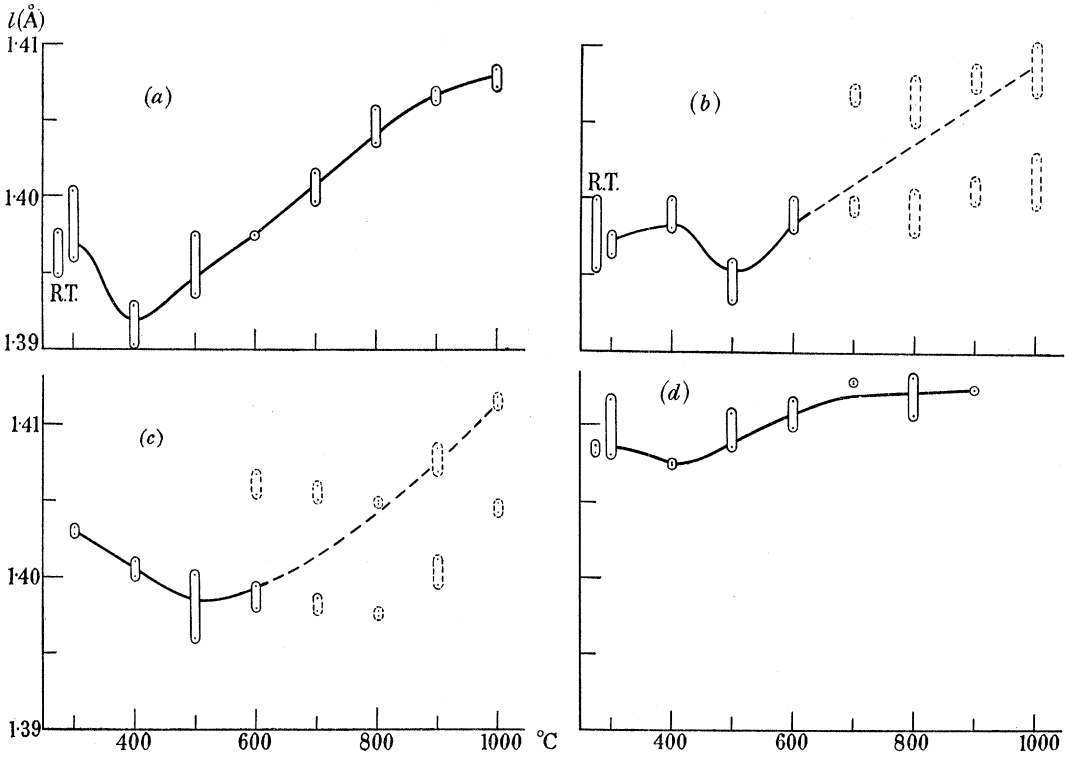

FIGURE 8. Variations in the mean C—C bond length within the layers. Two independent readings are shown for each temperature. *a*, Cannock Wood series; *b*, Meltonfield series; *c*, Roddymoor series; *d*, Pumpquart series.

Figure 8 shows the variations in mean C—C bond length within the layers. The method provides a measure of the bond length in terms of a fractional increment relative to the value assumed in calculating the $J(s)$ curves, (I), and used in the matrices, (II). Figures 8 (*b*) and (*c*) are earlier results than those of either (*a*) or (*d*), and were obtained with the use of matrices earlier than those published in II. In this earlier work, an attempt was made to match the assumed bond lengths to the values found elsewhere (e.g. by Donaldson & Robertson 1953) for molecules of similar size. Consequently, the significance of the measured fractional change in bond length depends on the sizes of the layers present in these cases, and in figures 8 (*b*) and (*c*) the line giving the implied bond length is shown broken where such an uncertainty exists. In figures 8 (*a*) and (*d*) there is no such uncertainty, since these results were obtained from the matrices of II in which a bond length of 1·405 Å was assumed for all size-groups.

In each of these four cases, a minimum is seen at 400 or 500 °C, depending on the starting material, the minimum being deepest with the lowest rank coal (Cannock Wood) and shallowest with the anthracite. In each case, except in that of the anthracite, the minimum comes just above the temperature at which the rate of evolution of volatile matter (weight %/°C) reaches a maximum, and is followed by an increase in bond length during the process of layer growth. Even in the anthracite, however, the bond length evidently stops short of the value for graphite (1·42 Å) by about 0·007 Å. For correlation purposes, the weight losses are also shown in figure 9.

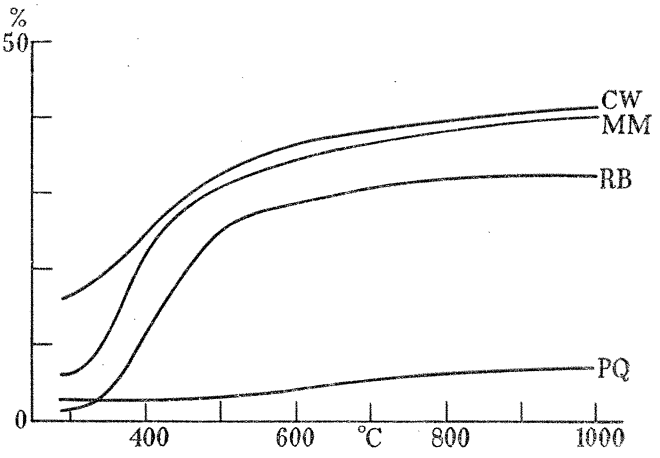

FIGURE 9. Weight losses during carbonization.

The random error (relative to the mean) of these measurements is of the order of 0·002 Å or less. The absolute error may also contain a systematic component of the same order of magnitude. All reasonable precautions were taken to ensure high accuracy, but a displacement of the diffraction pattern due to absorption in a specimen of finite diameter, and the possibility of film shrinkage during the *exposure* (but not during *processing*), may require these bond-length curves to be raised over-all by about 0·003 Å. The trends shown by the curves are, however, unaffected by this.

(*e*) *Comparison of observed and calculated intensities*

In this section we compare the observed and calculated intensities for values of s within, above, and below the working range.

Within the working range, no significant discrepancy between the observed and calculated curves has ever been found, except that which may be attributed to a small sideways displacement of one curve relative to the other due to a small residual error in the bond length. Root-mean-square errors within the working range have always been between 0·027 and 0·090 electron unit (about $\frac{1}{3}$ to 1 % of the mean intensity) which is about the accuracy required to obtain results of the consistency shown in figure 7 of II.

At higher angles, a systematic discrepancy has always been found, even for those specimens of the highest carbon content. The effect is a gradual drifting apart of the observed and calculated curves, the observed curve being some 4 % higher at $s = 1{\cdot}2$ Å^{-1}. This may mean either (i) that the theoretical data are too low at high angles, or (ii) that they are too high in the fitted range, or (iii) that the observed curve is subject to some form

of distortion. The recent work of Keating & Vineyard (1956) has confirmed that (ii) is the case, the error lying in the Compton scattering figures of Compton & Allison (1935). In addition to this effect, however, (iii) is operative because of absorption, and the polarization factor may also be imperfect. The correction of any error in the polarization factor (due to monochromator texture) would lower the observed curve at high angles. Figure 10 shows the comparison between observed and calculated curves throughout the range observable with Cu $K\alpha$ radiation, and in particular shows a number of curves in the high-angle region. These show that good agreement is obtained between the observed curve,

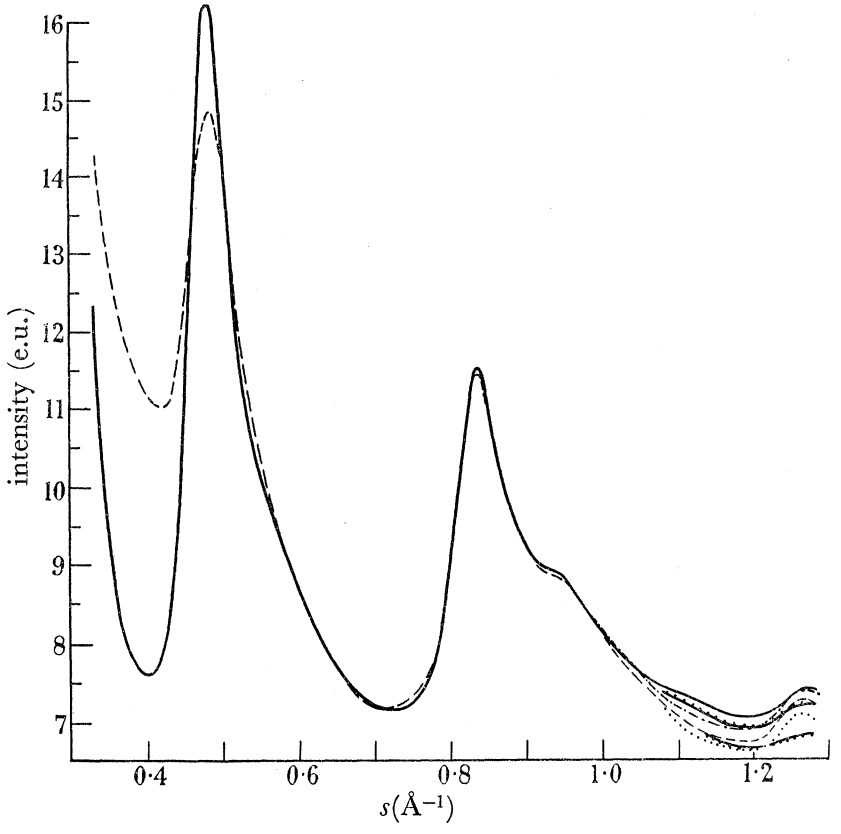

FIGURE 10. Comparison of observed and calculated intensities: ———, observed curve; ·····, observed curve with allowance for absorption, $\mu r = 0{\cdot}3$; ·····, observed curve with allowance for absorption, $\mu r = 0{\cdot}6$; — — —, calculated curve from Compton & Allison's figures, omitting B^{-3}; —·—·—, calculated curve from Keating & Vineyard's figures, omitting B^{-3}; · · · · ·, calculated curve from Keating & Vineyard's figures, including B^{-3}.

corrected for absorption with the product $\mu r = 0{\cdot}3$, and a curve calculated on the basis of Keating & Vineyard's figures with the Breit–Dirac* relativistic recoil factor omitted. On this basis, only a slight discrepancy, attributable to strain broadening (see below), persists at $s = 1{\cdot}25$ Å^{-1}. Fair agreement is also obtained between the observed curve, with μr assumed equal to 0·6, and a calculated curve obtained from Keating & Vineyard's figures including the Breit–Dirac factor, but the apparent strain broadening in this case seems excessive. Measurements made with Mo $K\alpha$ radiation, for which $\mu r = 0{\cdot}04$, are in good agreement with the unmodified observed curve, which supports the view that for

* The Breit–Dirac factor, by which tabulated Compton scattering figures should be multiplied before use, is the cube of the ratio of the X-ray frequencies in the primary and scattered beams (James 1948, p. 463).

Cu $K\alpha$ radiation, μr is not as high as 0·6 (which would imply an absorption coefficient more than twice that due to pure carbon). Mo $K\alpha$ measurements in the region $2{\cdot}0 \leqslant s \leqslant 2{\cdot}2$ Å^{-1} also show better agreement between observation and calculation if the Breit–Dirac recoil factor is omitted, and this is a region where the factor is important (*ca.* 10%) and rapidly changing; the gradient of the observed curve is found to differ from that of the calculated curve when this factor is included. Difficulties have also been encountered by others (P. B. Hirsch and J. D. Watt, private communications) in reconciling this factor with observation.

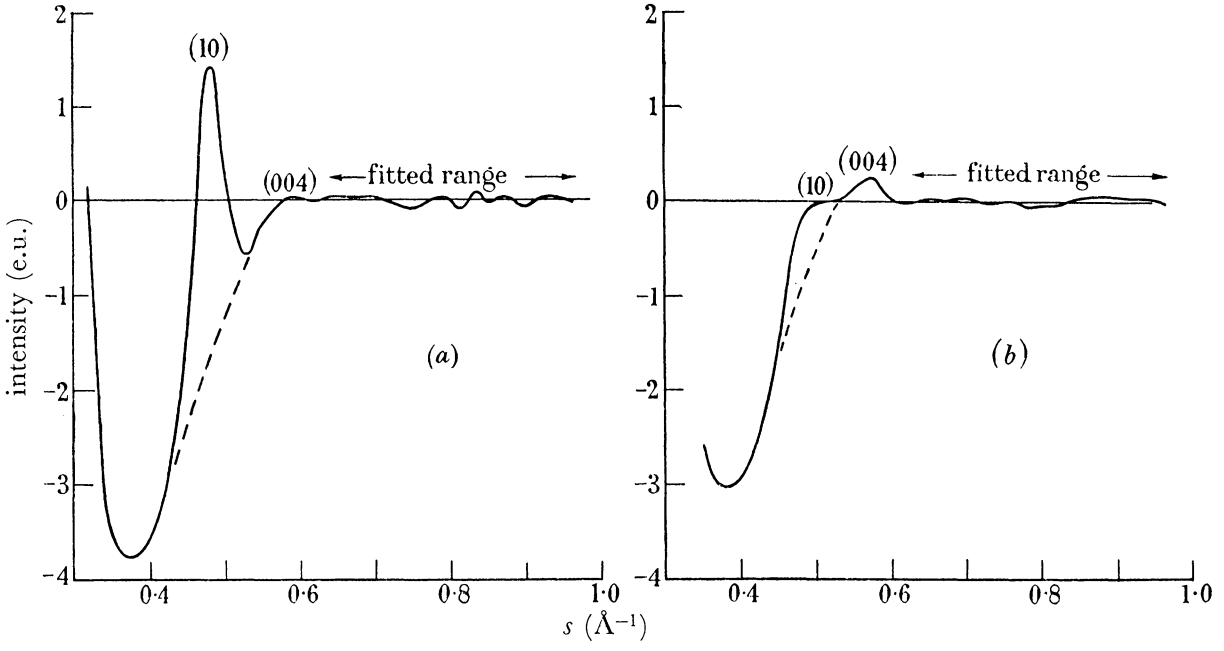

FIGURE 11. The difference $(I_o - I_c)$ between observed and calculated intensities for the Meltonfield 1000 °C; specimen (*a*) and Meltonfield 500 °C specimen (*b*). In each case the broken line is an interpolation representing the effect of the (00*l*) variation taken alone.

Below the working range ($s < 0{\cdot}66$ Å^{-1}) very important differences between the observed and calculated curves have always been found, as illustrated in figure 10. The difference between the two curves may be resolved into two parts. First, there is a difference due to the parallel stacking of the layers, which gives rise to variations of intensity along the line (00*l*) in reciprocal space, for which no allowance has been made in the theoretical curves used. For present purposes, the (00*l*) variation may be regarded as a heavily damped cosine wave oscillating about the mean value given by the theoretical intensity curves. The difference of some 3·5 electron units at $s = 0{\cdot}4$ Å^{-1} (for which $l = 3$) may be attributed entirely to the negative excursion of the (00*l*) variation at this point. In addition to this effect, there is also a genuine enhancement of the observed (10) peak relative to the calculated value, an effect which has previously been noted by Franklin (1950*a*). These two effects may be approximately resolved by interpolation when the intensity difference is plotted, as shown in figure 11.

The magnitude of the (10) discrepancy (i.e. that part of the intensity difference not attributable to the (00*l*) variation) has been investigated in several cases. For the Roddymoor and Meltonfield coals, (coking and caking coals, respectively) the difference appears

constant at about 0·8 e.u. up to 500 °C, whereas at 1000 °C, the discrepancy is in both cases about 3·0 e.u.

The following effects might be wholly or partly responsible for this discrepancy:

(i) Calculation shows that if the atomic scattering factor figures of McWeeny (1951) are regarded as correct, and those of Hoerni & Ibers (1954) (which were employed in the interpretation), as incorrect, then a net (10) discrepancy of from 0·25 to 0·5 e.u., depending on the layer size, may be attributed to a wrong choice of scattering factor. The atomic scattering factor cannot therefore be responsible for more than a small part of the discrepancy; furthermore, the discrepancy would be worse if the earlier figures of James & Brindley (1931) were regarded as correct (Franklin 1950*a*, Bacon 1952). Bacon (1952), in fact showed that for well-developed graphites, the discrepancy at the $(10\bar{1}0)$ peak vanished if McWeeny's figures for f are used, thus confirming their (and therefore also Hoerni & Ibers's) superiority over those of James & Brindley.

(ii) Calculation shows that if a temperature factor e^{-Ks^2} is applied to the oscillatory component of the diffraction function $J(s)$, a (10) discrepancy with just the right dependence on layer size may be produced provided the parameter K is unity. However, in §(*c*) (ii), we obtained an upper limit for K of 0·1, whence it follows that thermal vibrations are not responsible for more than a small part of the effect.

(iii) We may also dismiss the possibility of the establishment of three-dimensional (graphitic) order, since this has not been observed at preparation temperatures less than 1700 °C (Franklin 1951*a*), neither would it produce this type of discrepancy.

We therefore reach the important conclusion that some form of irregularity in the scattering layers is responsible for the effect. *Any* type of irregularity which involves the location of some atoms at sites close to, but not coincident with, positions corresponding to an extension of any nearby perfect, or near-perfect, hexagonal grouping of atoms, will suffice to produce a (10) discrepancy. The possibilities within this definition are obviously unlimited, but certain types of irregularity are more probable than others, and we will now consider three types.

(i) *Internal random effects*

If we assume that fluctuations in the C—C bond length introduce an uncertainty in the position of any atom in a layer relative to any other atom in the same layer, proportional to the separation of these atoms, then the function $J(s)$ of I should be replaced by

$$J'(s) = \Sigma \frac{n(r)}{N} e^{-\pi r^2 s^2 \tau^2} \frac{\sin 2\pi rs}{2\pi rs}. \tag{8}$$

For a layer of 20 Å diameter and with $\tau = 0{\cdot}1$, a theoretical intensity curve was obtained, which, when fitted to a calculated curve in the usual way, yielded a net discrepancy of 3·0 e.u. at the (10) peak, as do the two 1000 °C specimens mentioned above. Though there is reason to suppose that the τ value corresponding to the 1000 °C experimental cases is a little less than 0·1, and though there is no reason to assume that the relative uncertainties in atomic positions are proportional to their distance apart, rather than to the square root of this, or some other function, it is reasonable to take $\tau = 0{\cdot}1$ as representing the order of strain involved if the (10) discrepancy is to be explained on such a basis.

Now, such aromatic layers, provided they contain only carbon, are generally extremely regular, minor irregularities occurring only as edge effects (Donaldson & Robertson 1953), and an estimate of τ corresponding to the atomic positions given by Robertson & White (1945) for coronene is only 0·01; $\tau = 0{\cdot}1$ corresponds to a positional uncertainty of about 0·5 Å in 7 Å, the diameter of the coronene molecule. The magnitude of the strain required to account for the observed (10) discrepancy in terms of internal random effects is thus seen to be unreasonably large, and it is concluded that some other form of strain is primarily responsible.

(ii) *Edge groupings*

Any edge grouping bonded to the aromatic nucleus by bonds differing in length from those of the nucleus, or having inter-bond angles other than 120°, or having atoms not coplanar with the layer, will produce a (10) discrepancy. The simplest form of edge group, a single bonded —CH_3 group, has been studied quantitatively ((*c*) (iii) above) and it is found that such groups attached to layers of diameter 8·4 Å may produce a discrepancy of 0·1 e.u. at the (10) band, and a smaller discrepancy if they are attached to larger layers. More complicated edge groups must increase this figure, and it is considered likely that edge groups are the primary cause of the discrepancy of 0·8 e.u. found in the low-temperature specimens, but they are thought to contribute little to the discrepancy observed at the high temperature.

(iii) *Growth effects*

When two layers combine to form a larger layer, as is believed to take place during the carbonization process, there is every likelihood that, just after union, the two parts of the layer, though chemically bonded, are not perfectly alined relative to one another. They may be rotated relative to one another by a vacancy, or distorted by steric hindrance or some such imperfection introduced at the junction (as, for example, in the non-planar molecules discussed by Ubbelohde 1957); or they may not be co-planar, being bent along the junction line as in twinned graphite (Laves & Baskin 1956). After further heat treatment the latter type of imperfection may partially or wholly anneal out, in which case elastically curved layers may occur provided that their environment does not permit relaxation of the stresses involved.

In any of these cases, the lengths of inter-atomic vectors which span the junction (or the curved region in the last case) will differ from the corresponding perfect lattice values, and in these ways it is thought likely that the (10) discrepancy of 3·0 e.u. found in the high-temperature specimens may readily be explained by the presence of bent or curved layers of overall diameters of the order of 40 to 100 Å.

If such imperfections are present in the high temperature specimens, it is clearly necessary to reconsider the physical significance of the parameter L which is measured in this work. The X-ray scattering given by a bent layer, for example, is equivalent to that given by a planar layer of the same area at zero scattering angle, and approaches the weighted mean of the scattering from the two perfect regions as $(\sin\theta)/\lambda$ approaches infinity, being intermediate between these extremes in the working region of $(\sin\theta)/\lambda$. The approach to the latter extreme is the more rapid the more severe is the bend.

In paragraph (*c*) (iv) above it was shown that five-membered rings and hydroaromatic bridges are sufficiently severe departures from regularity for the latter extreme to be effectively reached at the position of the (11) band. No calculations have yet been carried out to ascertain the behaviour of such layers at the (10) band, though it is expected that here too, the latter extreme may be closer than the former. At the present time, therefore, the strongest categorical statement which may be made concerning observed L values is that they represent the upper limit of size of the perfect regions within larger layers which may contain junction defects, and that they are smaller than the lower limit of size of the larger imperfect regions; we must accept the measurements as representing what we may term equivalent perfect layers. Measurements of L based on the (10) band would represent the lower limit of size of the larger imperfect regions.

It is hoped to extend a quantitative study of the (10) band discrepancy a little further at some time, since the scattering from bent layers is calculable. It seems unlikely, however, that an unequivocal quantitative explanation of the (10) band discrepancy will be obtained, though a quantitative estimate of the magnitude of the defects involved, on the basis of a plausible model, is thought to be attainable.

4. Studies at low angles

(*a*) *Experimental technique*

In this part of the paper, we are concerned with the X-ray scattering occurring at s values $< 0{\cdot}4$ Å^{-1}. This range includes the (002) reflexion, which is always present and which is attributed to the parallel stacking of the layers; whilst the 'γ-band' (Blayden *et al.* 1944), the 20 Å band, and a central scattering maximum, may also be present, depending on the specimen. A qualitative description of the behaviour of these bands on carbonization has already been given by Cartz, Diamond & Hirsch (1956) and in more detail by Diamond (1956).

A symmetrical, transmission, Guinier-type camera was used to investigate this region (Guinier 1952, p. 166). The monochromator was LiF ground and plastically deformed to achieve line focusing, and the camera was evacuated.

The films obtained were measured in the same way as the high-angle films (§3(*a*)), except that no suitable fiducial mark was available at high angles, so that the inter-layer spacings quoted below may be subject to error from film shrinkage in processing. However, the camera radius was calibrated photographically using $NaClO_3$ as a standard, and a systematic error in the d spacing will therefore only be introduced if the calibrating film shrank by a significantly different amount from those subsequently taken from carbonized coals. (The lattice parameter of $NaClO_3$ was taken as 6·570 Å.)

The Perspex scale used to provide the s scale on the photometer charts, embodied, at the low-angle end, the results of Franklin's correction for the effects of the vertical divergence of the primary beam (Franklin 1950*b*).

In order to obtain $I(s)$, the measured intensity, I_m, should be multiplied by $\cos 2\theta$ (Guinier 1952, p. 256), and divided by the polarization factor, and two factors depending on the absorption in the specimen and in the film. The effect of absorption in the specimen may be expressed as

$$\frac{1-e^{-y}}{y} = 1-\frac{y}{2!}+\frac{y^2}{3!}-\frac{y^3}{4!}+\ldots, \qquad (9)$$

in which $y = t\ (\sec 2\theta - 1)$, which in practice varies between zero and 0·01, whence this correction is negligible. Hirsch (1953) concluded that the angular dependence of the absorption in the film is such as to make the combined effect of this and the polarization factor virtually independent of θ; thus $I(s)$ may be taken as $I_m \cos 2\theta$. Any errors introduced by this approximation are of little significance, provided that no quantitative comparison between the stacking of the layers and the groups responsible for the 20 Å band is attempted.

Two transforms are then derived as follows

$$P_1(z) = \int \frac{s^2 I(s)}{f^2} \cos 2\pi z s \, \mathrm{d}s \tag{10}$$

and

$$P_2(z) = \int \frac{I(s)}{f^2} \cos 2\pi z s \, \mathrm{d}s, \tag{11}$$

of which the first, when suitably normalized, gives the probability of finding a layer distant z from a given layer along the normal to the first layer; it thus represents a projection of the contents of Patterson space on to the normal to the layers at any given point in the specimen. This function is used to determine stacking distributions. The second function corresponds to a projection of the contents of Patterson space on to an arbitrary radius vector with random orientation, and is of value in studying textural effects, notably the 20 Å band.

For a detailed review of the theory of scattering in this angular range, the reader is referred to Cartz, Diamond and Hirsch (to be published) or Diamond (1956, chap. 12), in which 'cut-off', strain broadening and allied problems are discussed. Summaries of the double-difference method by which stacking distributions may be obtained have already been given by Hirsch (1953, 1954) and Diamond (1956, 1958*b*).

(*b*) *Results*

Figure 12 shows two series of stack-height distributions, obtained from calculations based on the assumption that the width of the (002) peak may be attributed entirely to 'particle-size broadening' and not to 'strain broadening', i.e. fluctuations in the inter-layer spacing within a given specimen are ignored. Cartz (private communication) has critically examined this assumption by analyzing difference curves of the type of figure 11, thus including the (004) reflexion in the transforms obtained. From these he concludes that substantial fluctuations in inter-layer spacing do occur, but have a very minor effect on the stacking distributions obtained, as is to be expected for such small stacks; this is equivalent to the statement that the (004) peak is attenuated relative to the (002), but with little change of shape.

The calculations leading to the results in figure 12 implicitly assume that there is no systematic tendency for layers of a particular size to be associated with stacks of a particular height. If this is not so, each term in the given distributions contains a weighting factor proportional to the mean area of the layers contained in stacks of the height in question.

These results are summarized in figure 13 which shows the mean number of layers per stack. The interesting variations shown therein are of the same form as those obtained by

Blayden *et al.* (1944), but correspond to stack heights of only ~ 10 Å, whereas their estimates for similar coals were considerably higher.

Transforms of $s^2I(s)/f^2$ have also been used to derive values of the inter-layer spacing, d. This is equal to the periodicity of the transform, but is not equal to the distance from the origin to the first maximum of the transform, nor even to the first point at which the transform is tangent to the upper branch of its envelope, owing to an apparent phase shift

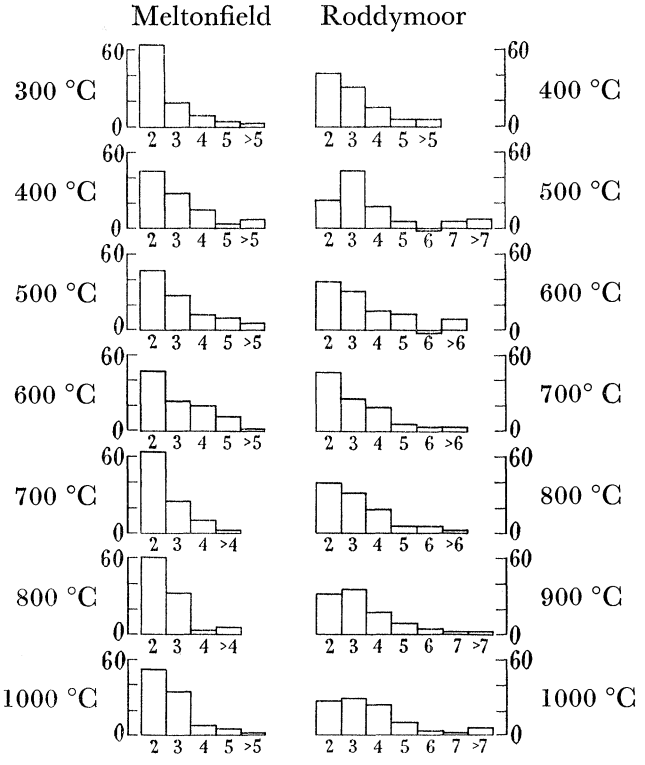

FIGURE 12. Stack-height distributions for the caking and coking coal series (left and right, respectively). The histograms give the percentage probability that a given stack contains n layers, n being the abscissa. Single layers are excluded from the calculation. Evidently, pairs and groups of three layers are the most common.

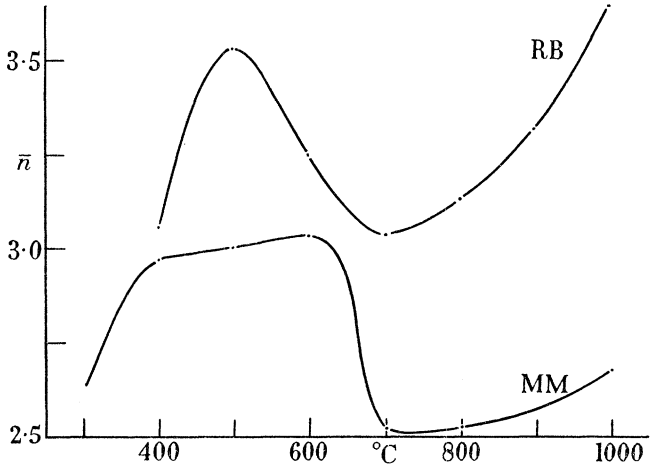

FIGURE 13. Mean number of layers per stack (excluding single layers from the average). $\bar{n} = \Sigma np/\Sigma p$ in which p is the probability of a stack of n layers.

at the origin associated with the very heavy damping of the oscillations of the transform. This point is discussed elsewhere, e.g. Diamond (1956), Cartz, Diamond & Hirsch (in preparation). Measurements of d are shown in figure 14 for the caking coal (Meltonfield series). Similar variations were also found for the coking coal, but as there is some doubt about the absolute values of the latter, they are not shown in the figure.

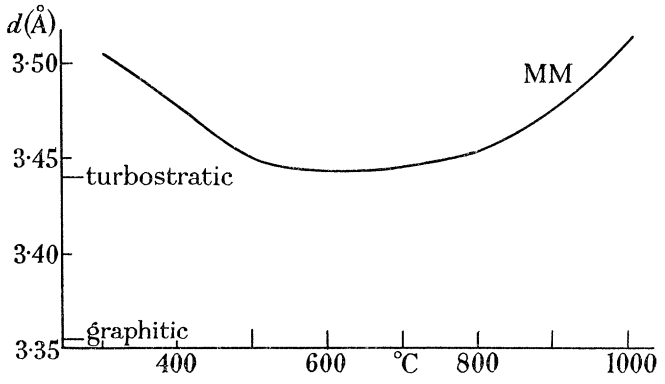

FIGURE 14. Measurements of the inter-layer spacing d, for the Meltonfield caking coal, compared to those found by Franklin (1951*b*) for turbostratic and graphitic carbons.

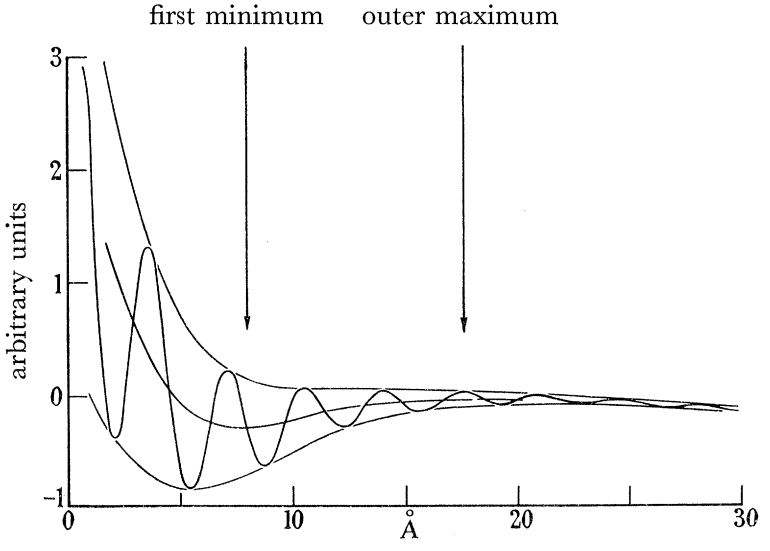

FIGURE 15. Transform of $I(s)/f^2$ for the Meltonfield 500 °C specimen.

A transform of the second type (equation (11)) is shown in figure 15. The transform consists of a number of ripples due to the layers (repeating at intervals of the inter-layer spacing) oscillating about a mean line which itself shows a pronounced minimum. The type of variation shown is the direct consequence of the presence of the diffraction maximum at 20 Å spacing, and may be interpreted in terms of scattering units such as that shown in figure 16, which has greater than average density in its core (necessarily approximating the graphite value of 2·2 g/cm^3 and *less than average* density in its peripheral regions. Such a scattering unit, with the dimensions shown, is consistent with all that is known about the sizes of the layers and their packing, for all cases where a 20 Å band has been observed, and, moreover, accounts for such a band without the need to postulate any systematically

preferred distance between the core regions of neighbouring units. The possibility of the existence of such a preferred distance is not, of course, ruled out. Outside the outer dashed circle in the figure, the structure is considered to be unrelated to the core in any systematic manner (although it may contain more such units); it follows that the average density in this region must be the mean for the specimen as a whole, and independent of the distance from the core, in agreement with the levelling out of the transform beyond about 20 Å.

The 20 Å band is of general occurrence in unheated vitrains having carbon contents between about 86 and 92%, being most pronounced at 89% C, and is thus typical of coking coals. It is therefore inferred that a preponderance of the structural units described

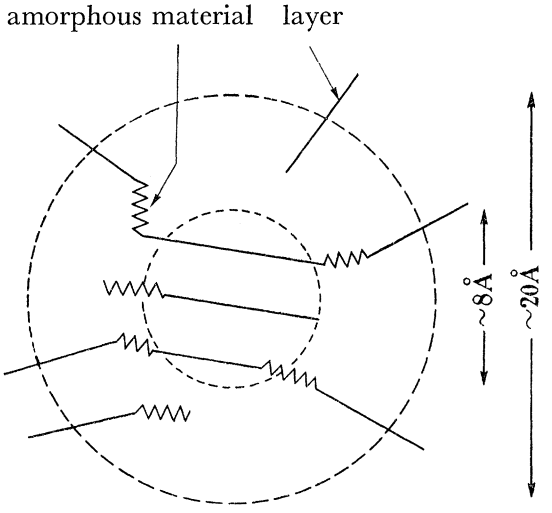

FIGURE 16. A scattering unit of the type believed to be responsible for the 20 Å band. (After Brown & Hirsch 1955.)

above (figure 16) makes up what may be termed a 'coking coal texture'. On this basis, the 'coking coal texture' is found to be developed by the caking coal at temperatures in the range 400 to 500 °C, although it is not conspicuous, if present at all, in the unheated specimens. At temperatures of 600 °C or higher, the groups responsible for the 20 Å band lose their identity by layer growth, and the 20 Å band gives place to diffuse low-angle scattering which (for temperatures of 700 °C or higher) increases monotonically with decreasing θ, indicating a wide distribution of pore widths and inter-pore distances.

5. Discussion and conclusions

In this final section, we bring together and discuss all the various trends and changes observed during the carbonization of the coals examined in this work. Central to this discussion are the results presented in table 3 and figure 6, and some comments on their significance follow.

First we note that the layer diameters of the unheated bituminous coals are extremely small, as was shown by Hirsch (1954). In the Cannock Wood series, the results for the 300 °C specimen, after allowance for the oxygen correction, show a distribution for the carbon alone so similar to figure 3*e*, that we may conclude that in this case the 5·8 Å term represents the only significantly populated aromatic size group.

A second fact emerges, and may be seen at a glance (figure 6), that for coals of less than anthracite rank, the temperature of treatment is a far more important variable than the rank of the starting material, at least so far as layer sizes are concerned.

The carbonization process is clearly seen as an evaporation of edge- and interstitial groups and of some heavily substituted aromatics of low molecular weight up to 500 °C, after which the differences between the three bituminous coals are quite minor, though differences in texture and degree of cross-linking remain. The differences of rank in the low temperature specimens appear primarily as differences in the amount of amorphous material present, with only comparatively minor differences in the sizes of the layers to which such material is attached. Measurements made by Dr L. Cartz on unheated coals fortify this statement, and also show the fraction of amorphous material estimated in this way to be similar in magnitude to estimates of the aliphatic carbon based on infra-red measurements (Brown & Hirsch 1955). But when the (admittedly extreme) 'corrections' for oxygen are made in the present work, it appears that in the oxygen-rich samples, the amorphous scattering actually observed is closely equal to the maximum which may be attributed to the oxygen alone (as single-atom scatterers), very little amorphous carbon being required to make up the difference. This suggests, but does not prove, that the amorphous scattering is truly made up of a term proportional to the oxygen content (the constant of proportionality being less than 1, and not equal to 1, as assumed in making the revisions) and that there is a genuine contribution proportional to the aliphatic carbon also. Such a situation would be entirely consistent with the results of § 3 (*c*) (iii) if phenolic or quinolic oxygen is present, and with the infra-red correlation just referred to.

With rising temperature, the removal of edge-groups by distillation leaves the remaining aromatic nuclei in a highly reactive condition and no longer insulated from one another, with the result that at higher temperatures suitably orientated neighbours coalesce to form larger layers. Some of the smallest layers, however, apparently fail to coalesce, and this is thought to be due to their unfavourable siting and misorientation with respect to their larger neighbours, whose positions and alining tendencies are increasingly the controlling influence.

The Pumpquart (anthracite) series, however, has a flying start over the others; not only does it have much less amorphous material initially, it also has a much higher degree of preferred orientation (Hirsch 1954; Brown & Hirsch 1955) which, as shown by Franklin (1951 *a*), greatly facilitates layer growth and subsequent graphitization by the favourable siting of neighbouring layers. Growth is apparently delayed by about 100 °C in this coal (figure 7), presumably because the larger layers present require greater thermal energy to allow them to move into position (Franklin 1951 *a*). When growth does set in, however, it goes at a much faster rate (Å/°C), which is readily interpreted as being due to the coalescence of larger layers. At 800 and 900 °C the smallest aromatic size group has almost entirely vanished, suggesting that, in contrast to the other coals, the preferred orientation in the raw coal is good enough to allow most of these to coalesce also.

Simultaneously with these changes, we observe interesting changes taking place in the ordered stacking of the layers in the Meltonfield and Roddymoor series. The changes indicated in figures 13 and 14 show clearly that as the amorphous material is evaporated away (below 500 °C), one of the obstacles to good packing of the layers is removed, and

the increased mobility of the layers is reflected in an increase in the mean number of layers per stack and in a decrease of 0·05 Å in the inter-layer spacing. When layer growth sets in, however, the layers are attacked at their edges, and the formation of larger layers (now the dominant process) leads to a reduction in the number of layers per stack by drawing the layers out sideways (figure 13, 700 °C).

At still higher temperatures, the packing improves again, since the larger layers now formed have a stronger tendency to stack parallel to one another than the previously existing small layers. In the high temperature range, also, the inter-layer spacing increases again (figure 14). The reason for this is less clear, but it is thought to be due to possible conflict between cross-links at the edges of such layers and to fragments 'in the way' of the larger layers, preventing them from coming together properly. The minimum value of the interlayer spacing found for the Meltonfield series, when the packing is at its best, is closely equal to that found by Franklin (1951 *b*) for turbostratically packed carbons (3·44 Å), in accordance with the view that in the middle temperature range *ca.* 500 to 600 °C), there are fewer impediments to the packing tendency than in any other range below 1000 °C.

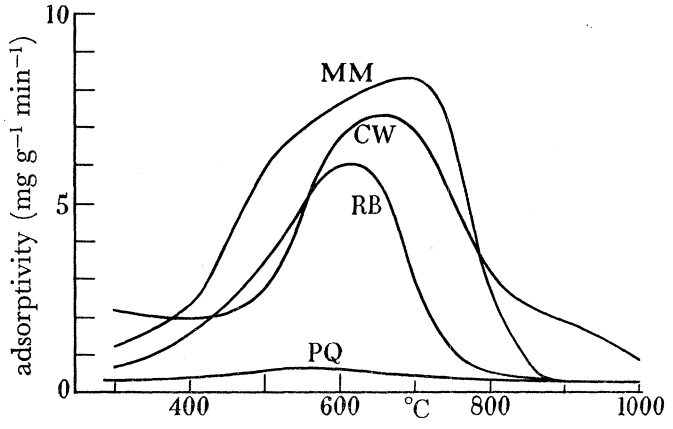

FIGURE 17. Mean rate of gain of weight immediately after releasing the furnace vacuum.

In addition to these effects, we observe interesting variations of texture and 'adsorptivity'. A semi-quantitative measure of the adsorptivity was obtained by noting the mean rate of gain of weight of the carbonized specimens during the first 10 min after breaking the furnace vacuum, at which time some of the specimens adsorbed atmospheric gases at a rate measurable in milligrams per gram per minute. Graphs of this quantity are shown in figure 17. Brown & Hirsch (1955) were the first to describe the scattering units which are associated with the 'coking coal texture' (figure 16). In their paper, the development of this texture finds a close correlation with a reduction in the amount of cross-linking by hydrogen-bonded phenolic OH groups in particular. Brown (1955) not only finds that the infra-red spectra of a coking and a caking coal differ in that the latter shows evidence of such hydrogen bonds where the former does not, he also finds that the evidence for these bonds vanishes on carbonization between 400 and 500 °C, which is just the range in which the Meltonfield caking coal develops the 'coking coal texture'.

Now in the carbonization of the Meltonfield caking coal, the changes that take place up to 500 °C are seen as a removal of groupings from the peripheral regions of stacks such as that shown in figure 16, and improved adjustments in the stacking, thus increasing the

contrast in density between core and periphery, and introducing the coking coal texture with its associated band at 20 Å. The hydrogen bonded OH groups which disappear (or at least cease to be hydrogen bonded) in this range, are thought to play a part in the connexion of the amorphous material to the aromatic layers and in the cohesion of the whole; and in particular, they are thought to be responsible for the fact that the coking coal (free from such bonds) melts completely at about 420 °C, whereas the caking coal only softens, its layers being rendered less mobile by the hydrogen bonds and other forms of cross-linking.

This process is also suggested by the results shown in figures 9 and 17. The removal of volatile material (figure 9) proceeds at a maximum rate at 400 °C during the formation or enhancement of the coking coal texture, and in the later stages of 'degassing' (*ca.* 550 °C), when more firmly held material is evaporated, the breaking of the bonds by which such material was held leaves the sites from which it comes in a highly reactive state, as indicated by the maximum adsorptivity shown for all coals at about 600 °C and by the concentration of free radicals (see below). This maximum clearly follows the evolution of volatile material very closely.

As the temperature rises further and growth by coalescence sets in, the adsorptive capacity of the product falls catastrophically, due partly to the satisfaction of the reactive sites by growth, and partly to a reduction in the accessibility of the remaining sites brought about by the movements and formation of large layers. The porosity, however, continues to rise throughout the range, as is shown by the marked increase in very low-angle scattering, and by density measurements made in liquids and in helium (Franklin 1949).

The fact that the anthracite shows very little adsorptivity and yet is highly porous, is presumably due to the fact that only a little material is volatilized (thereby leaving comparatively few reactive sites) and to the closed nature of the pore system.

The phenomenon of paramagnetic resonance is also observed in coals carbonized at temperatures less than 700 °C, with a strong maximum in the effect at 550 °C (Ingram *et al.* 1954; Bennet *et al.* 1955; Ingram 1957). By varying the frequencies employed, these authors were able to show that the mechanism responsible for this resonance is not associated with graphitic conduction electrons (as may be the case with specimens carbonized at much higher temperatures), but may be attributed to electrons having unpaired spins, such as may be produced by the destruction of covalent single bonds between the aromatic layers and the edge groups undergoing volatilization. The resonance develops in just the temperature range in which the destruction of such bonds is believed to be taking place, has its maximum where this is largely complete (550 °C) and where the 'coking coal texture' is best developed, and vanishes again when the free radicals so formed pair off their spins by reacting with neighbouring layers during coalescence.

The production of free radicals in this way results in an unpaired electron on the atom from which a bond has been broken; and though such electrons are unable to migrate far from their parent atoms for electrostatic reasons, it seems reasonable to suppose that they are available to increase the bond order of the aromatic bonds in the neighbourhood of such atoms, and such an increase would result in a decrease in bond length (Pauling & Brockway 1937). Now the present measurements of bond lengths, with the exception of the anthracite, show just such a minimum in the bond length—occurring at 400 °C for the

Cannock Wood series, 500 °C for the Meltonfield series and between 500 and 600° C for the Roddymoor series. In each case these temperatures are close to the shoulder of the corresponding weight-loss curve (figures 8, 9).

Qualitatively, therefore, the bond length and resonance measurements are consistent with the mechanism described. Quantitatively, however, the bond-order increase is found to be inadequate to account for the observed fall in bond length; one free electron to every twelve aromatic carbon atoms would be required to account for the drop of 0·005 Å found in the Cannock Wood case, as might arise from the removal of one edge group from each layer. Ingram *et al.* (1954) estimated the presence of one free radical per 1600 carbon atoms at 550 °C, which is only a hundredth of the figure estimated from the bond length. Even if there is a partial repairing of the free electrons produced (thus rendering them detectable to X-rays but not to resonance experiments), or if the comparision is influenced by the presence or absence of atmospheric oxygen at the time of measurement, it still seems unlikely that a factor of 100 would be introduced.

But there is another, more direct, effect which influences the bond length measurement. It was reported (§3 (*c*) (iii)) that first atoms of aliphatic side chains contribute totally to the apparent size of the layer to which they are attached, and therefore the bonds linking such atoms to the aromatic nuclei must influence the effective mean bond length of the group as a whole (though with much less than unit weight) and the lengths of such bonds approach the aliphatic C—C distance of 1·54 Å rather than the lower aromatic values. Examination of the theoretical data used for the work of §3 (*c*) (iii) showed that the removal of edge-groups from about a third of the available sites would be sufficient to account for the observed drop of 0·005 Å, i.e. desubstitution to the extent of two or three edge groups per layer.*

Both the above mechanisms are thought to be operative, the latter being the major effect.

As growth of the layers sets in, the mean bond length approaches the graphite value of 1·42 Å, in general accordance with expectation.

The anthracite results are also readily understood. The presence of large layers in the raw coal is, no doubt, responsible for the much larger bond length observed in this case, and the absence of a distinct minimum in the bond-length curve correlates perfectly with the much reduced volatilization compared with the bituminous series. As in other coals, the onset of layer growth is accompanied by an increase in bond length, the value of 1·412 Å being attained at 900 °C.

Thus, while the variational trends displayed by the bond-length measurements are quite accountable (and independent of systematic errors), their absolute magnitudes, even after allowing for the estimated maximum systematic error given at the end of §3 (*d*), are uniformly lower than might be expected by *ca.* 0·005 Å. It is difficult to be

* If, however, phenolic C—O or quinolic C=O bonds are broken during distillation, their effect will be slightly to counter the drop in mean bond length due to the destruction of C—C bonds, since these phenolic and quinolic bonds are both shorter than the aromatic C—C distance. However, the aliphatic C—C bonds differ in length from the aromatic bonds by +0·14 Å, whereas the phenolic and quinolic bonds differ by −0·04 and −0·18 Å, respectively. Phenolic bonds have therefore very little weight in this respect whilst the quinolic bonds are comparatively rare. It is not surprising, therefore, that the influence of the aliphatic C—C bonds predominates in the observed effect, and they alone are taken into account in main discussion.

PHILOSOPHICAL TRANSACTIONS OF THE ROYAL SOCIETY A MATHEMATICAL, PHYSICAL & ENGINEERING SCIENCES

categorical about the significance of this, but in the high temperature cases, where the existence of substantial bending or buckling of the layers is established, the measured bond length must be influenced to some extent by C—C vectors which are shorter than their ideal (flat layer) values on account of the non-planarity of the layer. The measured bond length, however, does not simply correspond to the mean scale of the projection of such a layer on to its mean plane, since the influence of the longer vectors, which are most affected by such foreshortening, will only be felt if the foreshortening is slight enough for these vectors to retain approximate phase coherence with the shorter vectors in contributing to the diffraction function $J(s)$. If such phase coherence is not even approximately retained, such vectors will contribute in random phase to $J(s)$ and will not be effective in determining the position of the (11) peak, in which case they cannot influence the bond

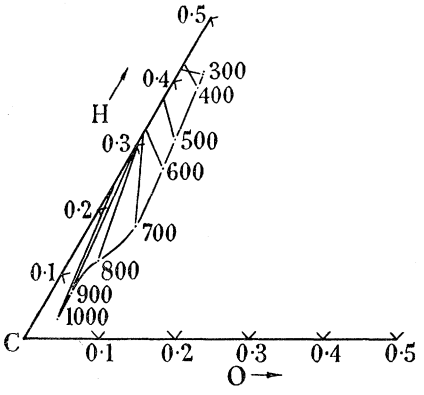

FIGURE 18. Atomic abundance ratio diagram for the Roddymoor series. Points on the full line represent the compositions found, in which O is obtained by difference and other elements are neglected. For an explanation of the tie-lines see text. The ratios are by number, not weight.

length measurement either. (For example, a C—C vector 30 Å long, when foreshortened by $\frac{1}{3}$% relative to its flat-layer value, will contribute to $J(s)$ a term $(\sin 2\pi rs)/2\pi rs$ which is already 30° out of phase at the (11) band). If, however, the reduction of 0·005 Å relative to the expected values is to be explained on such a basis, it may be borne in mind that a bond of length 1·405 Å will appear foreshortened by this amount if projected through an angle of 4·5°.

We come now to consider the nature of the small molecules which evidently persist in the bituminous series at temperatures right up to 1000 °C. The suggestion that such layer fragments are genuine, generally meets with the objection that their presence would require a great deal of hydrogen to be present in order to satisfy their edge valencies.

If we suppose the layers present to be bounded by hydrogen atoms and chemically independent, then the atomic abundance ratio H/C is approximately given by $3/L$ (L in Å) for each size group. Thus, when the population of each size group is known, the value of H/C required by the specimen as a whole, in order to satisfy the valencies on the periphery of the layers, may be calculated. Such 'free layer' compositions have been calculated in each case, and the values for the Roddymoor series are marked (along the C—H edge) of the atomic abundance ratio diagram of figure 18. (For the purpose of these calculations the amorphous material has been treated as CH_2.) Each 'free layer' composition is connected by a tie-line to the point representing the composition found for the specimen in question.

At low temperatures, even in the anthracite (not shown), the compositions are approximately consistent with the free layer model. At higher temperatures, however, this is far from true; the lengths and directions of these tie-lines indicating that the perfect regions of the graphitic layers, whose sizes are measured by X-rays, are not generally bounded by hydrogen atoms, but by chemical links to similar regions to form composite layers in the manner suggested in §3(*e*). In the Roddymoor 1000 °C specimen, for example, the free layer model could not occur unless the average of $1/L$ is 1/100 Å^{-1}.

It is, in fact, difficult to see how growth of the layers could take place without such a situation arising. Layers coming together to coalesce must first free themselves of obstructing hydrogen atoms, and must be approximately correctly alined; they must then form their chemical links (not all of which will be formed at one temperature, presumably) and must finally trim their alinement before they will appear as a large layer. This last stage may involve considerable movements perpendicular to the planes of the layers involved, to which the impedance must be large. It is to be expected, therefore, that specimens cooled from any given temperature ($\geqslant$ 700 °C) will contain layers in such intermediate stages of coalescence, which would account simultaneously for the hydrogen shortage and the surplus of intensity at the (10) peak already discussed.

Now what of the smallest layers? There appear to be two possible explanations of these. The first is that the smallest layers are some which are caught badly out of alinement with those that coalesce, and which therefore succeed only in cross-linking to the bigger layers and not in adjusting their alinement also. By cross-linking, they reduce their own mobility, and, as the bigger layers continue to grow, the influence of the smaller layers on the changes that take place becomes less significant: both these factors would tend to further handicap the growth of these retarded layers. The existence of small layers in this condition may also provide the cross-linking held by Franklin (1951*a*) to be responsible for the non-graphitizability of chars prepared from bituminous coals at higher temperatures.

The second possible explanation of these small layers is to be found in the possible existence of small holes in the larger layers, which may be introduced when badly fitting layers coalesce. The work of §3(*c*)(v) shows that such holes result in the appearance of a term corresponding to the size of the holes, and in a compensating depression of those terms which correspond to sizes intermediate between those of the holes and of the layer. The bi-modal nature of the histograms obtained at the upper temperatures is perfectly consistent with the existence of this effect. However, holes in the middle of large layers leave carbon atoms at the inner edges whose valencies are less easily satisfied by cross-linking, and which would otherwise require nearly as much hydrogen as a free layer of the same size. It is probably also significant that the persistence of very small layers is not observed in the Pumpquart series where the higher degree of preferred orientation present in the raw material facilitates the coalescence of all layers, so that the small ones do not get left behind and the resulting product is graphitizable. These last two considerations, together with the steadiness of the 5·8 Å term in the bituminous series, tend therefore, to favour the first interpretation, that fragmentary layers of the smallest size really do exist in a heavily cross-linked condition, though the existence of the hole effect remains a possibility.

Finally, it is worth making the point, shown very clearly by the histograms for the Roddymoor series, that as growth takes place and the right-hand maximum moves towards

larger sizes, the maximum representing the smallest layers does no such thing. If this small-layer term were an artifact arising from some peculiar strain distribution in the larger layers, then the undoubted growth of the larger layers would be expected to produce comparable changes in the terms representing the smaller groups, if these are in any way ghost terms; this fact alone suggests that these terms are genuine.

6. Summary

The main results of this investigation are as follows. In the bituminous coals, heat treatment causes an expulsion of volatile groupings from the peripheral regions of small clusters of two or three more or less parallel layers of carbon atoms, and this process is followed by the coalescence of the residual layers to form larger sheets which contain distortions believed to originate at the junctions. Changes in the mean C—C bond length, in the numbers of layers associating to form a stack, and in the distance separating these layers, accompany the above process and are interrelated in the manner described in the discussion section. In these coals also, the layer-size distribution depends more on the temperature of carbonization than on the rank of the starting material.

In the anthracite studied, the initial distribution of layer sizes is much wider and the tendency for these layers to be oriented parallel to the geological bedding plane is much greater. These facts result in an accelerated layer growth (though with a higher threshold temperature) and (unlike the bituminous series) in a growth process which involves virtually all the layers present. The much reduced volatilization results in a very much smaller reduction in the C—C bond length in the neighbourhood of 500 °C.

I am pleased to acknowledge my great indebtedness to Professor Sir Lawrence Bragg, F.R.S., Professor N. F. Mott, F.R.S., and Dr W. H. Taylor for much encouragement and for the provision of laboratory facilities; to Dr P. B. Hirsch for countless discussions and suggestions, especially in relation to interpretative questions; to the Director and staff of the University Mathematical Laboratory, Cambridge, for the use of many facilities, especially the EDSAC for the least-squares computations and the Hollerith punched card machine for the Fourier transformations; to my colleague Dr L. Cartz for his close and willing co-operation throughout; to Mrs J. Blows and Mrs D. Affleck (especially the former) for the greater part of the routine computational work; to Mr C. E. Chapman and his assistants for the maintenance and service of equipment upon which such work as this depends; to Dr G. W. Fenton of the Coal Survey Laboratory, Sheffield, for the provision of all the raw specimens; and Drs Weiler and Strauss of the Micro-Analytical Laboratory, Oxford, for the chemical analyses.

Finally, I am most indebted to the National Coal Board for their financial support and continued interest in the work; and to Sir Charles Ellis, F.R.S., on whose suggestion the work was initiated.

PHILOSOPHICAL TRANSACTIONS OF THE ROYAL SOCIETY A MATHEMATICAL, PHYSICAL & ENGINEERING SCIENCES

References

Bacon, G. E. 1952 *Acta Cryst.* **5**, 492.

Bangham, D. H., Franklin, R. E., Hirst, W. & Maggs, F. A. P. 1948 *Coal Res.* **7**, 153.

Bennett, J. E., Ingram, D. J. E. & Tapley, J. G. 1955 *J. Chem. Phys.* **23**, 215.

Blayden, H. E., Gibson, J. & Riley, H. L. 1944 *Proceedings of a Conference on the Ultra-Fine Structure of Coals and Cokes*, p. 176. London: British Coal Utilisation Research Association.

Brown, J. K. 1955 *J. Chem. Soc.* p. 752.

Brown, J. K. & Hirsch, P. B. 1955 *Nature, Lond.* **175**, 229.

Cartz, L., Diamond, R. & Hirsch, B. P. 1956 *Nature, Lond.* **177**, 500.

Compton, A. H. & Allison, S. K. 1935 *X-Rays in theory and experiment.* London: Macmillan.

Diamond, R. 1956 Ph.D. dissertation, University of Cambridge.

Diamond, R. 1957 *Acta Cryst.* **10**, 359.

Diamond, R. 1958*a* *Acta Cryst.* **11**, 129.

Diamond, R. 1958*b* *Proceedings of the Third Conference on Carbon*, University of Buffalo, June 17–21, 1957, London: Pergamon Press.

Donaldson, D. M. & Robertson, J. M. 1953 *Proc. Roy. Soc.* A, **220**, 157.

Franklin, R. E. 1949 *Trans. Faraday Soc.* **45**, 668.

Franklin, R. E. 1950*a* *Nature, Lond.* **165**, 71.

Franklin, R. E. 1950*b* *Acta Cryst.* **3**, 158.

Franklin, R. E. 1951*a* *Proc. Roy. Soc.* A, **209**, 196.

Franklin, R. E. 1951*b* *Acta Cryst.* **4**, 253.

Guinier, A. 1952 *X-Ray crystallographic technology.* London: Hilger and Watts.

Hirsch, P. B. 1953 The structure and texture of coal, 5th Report to the National Coal Board.

Hirsch, P. B. 1954 *Proc. Roy Soc.* A, **226**, 143.

Hoerni, J. A. & Ibers, J. A. 1954 *Acta Cryst.* **7**, 744.

Ingram, D. J. E., Tapley, J. G., Jackson, R., Bond, R. L. & Murnaghan, A. R. 1954 *Nature, Lond.* **174**, 797.

Ingram, D. J. E. 1957 *Proceedings of a conference on industrial carbon and graphite* (London 24–26 Sept.) to be published.

James, R. W. 1948 *The optical principles of the diffraction of X-rays.* London: G. Bell and Sons Ltd.

James, R. W. & Brindley, G. W. 1931 *Phil. Mag.* **12**, 81.

Keating, D. T. & Vineyard, G. H. 1956 *Acta Cryst.* **9**, 895.

Laves, F. & Baskin, Y. 1956 *Z. Krist.* **107**, 337.

McWeeny, R. 1951 *Acta Cryst.* **4**, 513.

Pauling, L. & Brockway, L. O. 1937 *J. Amer. Chem. Soc.* **59**, 1223.

Robertson, J. M. & White, J. G. 1945 *J. Chem. Soc.* p. 607.

Ruland, W. 1959 *Acta Cryst.* **12**, 679.

Ubbelohde, A. R. 1957 *Nature, Lond.* **180**, 380.

Wilson, A. J. C. & Lipson, H. 1941 *Proc. Phys. Soc.* **53**, 245.

PHILOSOPHICAL TRANSACTIONS OF THE ROYAL SOCIETY A MATHEMATICAL, PHYSICAL & ENGINEERING SCIENCES